Abstract

Objectives: The exact aetiopathogenesis of microdamage induced long bone fractures remains unknown. These fractures are likely the result of inadequate bone remodeling in response to damage. This study identifies an association of osteocyte apoptosis, the presence of osteocytic osteolysis and any alterations in sclerostin expression with fracture of the third metacarpal bone of (Mc-III) thoroughbred (TB) racehorses.

Methods: 30 Mc-III bones were obtained; 10 from bones fractured during racing, 10 from the contralateral limb and 10 from control horses. Each Mc-III bone was divided into fracture site, condyle, condylar groove and sagittal ridge. Microcracks and diffuse microdamage were quantified. Apoptotic osteocytes were measured using TUNEL staining. Cathepsin K, matrix metalloproteinase -13 (MMP-13), HtrA1 and sclerostin expression was analysed.

Results: In the fracture group microdamage was elevated 38.9±2.6% compared to controls. There was no difference in osteocyte number and % of apoptotic cells between contralateral limb and unraced control, however, there were significantly less apoptotic cells in fractured samples ($p<0.02$). Immunohistochemistry showed that in the deep zones of the fractured samples sclerostin expression was significantly higher ($p<0.03$) of the total number of osteocytes. No increase in cathepsin K, MMP-13 or HtrA1 was present.

Conclusions: There is increased microdamage in Mc-III bones that have fractured during racing. In this study this is not associated with osteocyte apoptosis or osteocytic osteolysis. The finding of increased sclerostin in the region of overt fracture suggests that this protein may be playing a key role in the regulation of bone microdamage during stress adaptation.

Article summary

Article focus

This study identifies evidence for non-apoptotic bone remodelling mechanisms by osteocytes in microdamaged bone.

Secondly this study investigate whether the wnt signaling protein sclerostin is altered in fractured bone.

Key messages

This study found that targeted remodelling in the bone is not dependent on osteocyte apoptosis.

The key finding is a marked increase in the wnt signalling inhibitor sclerostin, suggesting that this protein may be produced at sites of high bone density to reduce further bone deposition playing a key role in the regulation of bone microdamage during stress adaptation.

Strengths and limitations of this study

This study has strong clinical sample size (n=30) of distal Mc-III bones both fractured and non-fractured Thoroughbred horses.

This study indicate that microdamage in the racehorse has a fundamentally different pathological process to that modelled in small rodent animals and these results should be further validated in human fracture model.

Introduction

Long bone fractures in horses have significant welfare and economic implications to the horseracing industry. Key to the prevention of fractures is a clear understanding of their aetiopathogenesis. In horses, long bone fractures occur either due to a one off overload incident or due to repetitive microdamage and subsequent weakening usually associated with high intensity exercise. Fractures resulting from microdamage are commonly termed ‘stress fractures’ and often present as catastrophic fractures at exercise (1). In the UK the most recent study of days lost from training by two or three year old Thoroughbred (TB) horses showed that lameness was the most important cause of lost training days. Stress fractures were the most important cause of lameness, with an incidence of 1.48 and 1.43/100 per horse months in 2 and 3 year old horses respectively (2, 3). A number of bones are affected by stress fracture, including the carpal bones, proximal sesamoid bones, tibia and humerus with the distal condyle of the third metacarpal bone (MCIII) being one of the most common sites affected (4, 5).

The TB racehorse runs at speeds exceeding 15 m/s, applying highly repetitive surface strains of >5000με to MCIII (6) which leads to microdamage accumulating in the joint surface and adjacent subchondral bone plate (7, 8). This damage is observed to have distinct two histological forms, linear microcracks or diffuse microdamage (9-11). During these high intensity exercise regimes, a process of ‘targeted bone remodelling’ is used to repair

the microdamage (12). Bone remodelling in the body requires the coupling of bone resorption and formation and occurs to maintain mineral homeostasis, to adapt to mechanical change and to repair damage – the latter two scenarios are site-specific and are termed ‘targeted remodelling’ (12).

Stress fracture is likely a result of inadequate targeted remodelling in response to microdamage, when bone resorption exceeds bone formation, leading to weakened bone and overt fracture lines are propagated. Targeted remodelling is controlled by osteocytes (13) that have a number of key roles in bone homeostasis, including the regulation of bone formation, the control of bone resorption via both apoptotic and non-apoptotic pathways, RANKL mediated signals and the transduction of mechanical signals to induce an appropriate biological response (13, 14). The regulation of bone formation by osteocytes is predominately via sclerostin production, a wnt signalling inhibitor that inhibits bone formation (15) and is modulated by local load (16)). Inhibition of sclerostin with neutralizing antibodies has also been shown to speed up fracture healing (17) and sclerostin knockout mice have been shown to have faster fracture healing (18), providing evidence that sclerostin may inhibit bone healing *in vivo*. Non-apoptotic mechanisms of bone remodelling include direct remodelling of the perilucunar bone (‘osteocytic osteolysis’) (13). Osteocytic osteolysis takes place via the production by osteocytes of degradative enzymes, such as Cathepsin K (19), MMP 13 (20) and the serine protease HtrA1 (21) as well as the classic osteoclast enzyme, TRAP, and

these enzymes can be used as surrogate markers for this process. However, whilst some studies in the TB have investigated the role of osteocytic apoptosis in stress fractures, no studies have been performed in horses to investigate wnt signalling pathways or direct remodelling in microdamaged bone.

This study identifies evidence for non-apoptotic bone remodelling mechanisms by osteocytes in microdamaged bone and to investigate whether the wnt signaling protein sclerostin is altered in microdamaged bone.

Methods

Animals Third metacarpal (Mc-III) bones were obtained from Thoroughbred racehorses that were euthanased as a result of catastrophic fracture on the racetrack in California, U.S.A. and collected as part of the California Horse Racing Board post-mortem programme (Figure 1). The study groups were as follows: Group F distal Mc-III lateral condylar fractures that occurred on the racetrack immediately prior to euthanasia (n=10), Group CL (n=10) distal MC-III contralateral (uninjured) leg from horses in Group F (n=10). Horses with bilateral fractures were excluded as where those with concurrent fracture pathology. Group C distal Mc-III obtained from Thoroughbred horses that had sustained fatal non-orthopaedic injuries on the racetrack (n = 10). For Groups F and CL the horse mean age was 4.1 +/- 1.2 years, for Group C the horse

mean age was 3.9 +/- 1.5 years. For all samples, distal thoracic limbs were transected at the level of the carpal bone and stored at -20 ºC after humane euthanasia.

Specimen preparationA dorso-proximal palmaro-distal frontal plane bone block of the distal Mc-III (22, 23) approximately 1 cm thick was prepared using a band saw. The bone block of the joint surface was then divided into four pieces using sagittal plane cuts to create separate blocks of each of the regions-of-interest: lateral condyle fracture site, medial condyle, medial condylar groove and sagittal ridge (23) (Figure 2).

Preparation of tissue sections For each site both frozen and polymethylmethacrylate (PMMA) sections were obtained. Frozen samples were subsequently used for immunohistochemistry, PMMA samples for histological staining. Frozen sections were produced by embedding with OCT Cryoembedding Compound (SDLAMB/OCT, Fisher) and snap-freezing in liquid nitrogen. Sections of 10 µm thickness were made through the central portion of the bone block using a crysotat. The unfixed and non-demineralized tissue cryosections were tape transferred and glued to slides with UV sensitive glass adhesive. PMMA sections were obtained as follows. Bone blocks were fixed in 70% ethanol and bulk-stained in 1% basic fuchsin (JT Baker® Basic Fuchsin, JTB-B660-03, SureChem Products Ltd) in a graded series of ethanols (80%, 90%, 100%) for a total staining time of 18 days

allowing thorough penetration of stain and dehydration of the bones. After embedding in PMMA, 20 μm calcified oblique frontal plane sections were prepared from the centre of each block. This basic acid Fuchsin technique stains microcracks and diffuse matrix damage that existed before histologic sectioning (24).

Visualisation of microdamage PMMA sections were dehydrated, mounted in DPX mounting medium (44581, Sigma) and dried. Sections were imaged using a Fluorescence Microscope (Leica, DMRB) and over 200 microscope images per section were stitched together using Surveyor image analysis software and subsequently analysed with ImageJ software. The number of microcracks were quantified by expressing the number of cracks per section normalized to the total length of the cartilage/subchondral bone interface for each section. Branched cracks were counted as one crack and each section was scored blind by the same observer to ensure consistency between data collection. Diffuse damage was quantified by expressing the number of discrete areas of diffuse damage section normalized to the total length of the cartilage/subchondral bone interface for each section.

Quantification of osteocyte apoptosis The prevalence and location of apoptotic osteocytes/osteoblasts was detected using The DeadEnd™ Fluorometric TUNEL System (G3250, Promega).

Briefly, the cryosections were fixed by immersing slides in freshly prepared 4% methanol-free formaldehyde solution in PBS (pH 7.4) for 5 minutes at room temperature. The slides were washed by immersing in PBS for 5 minutes. Incubation in Proteinase K solution (20µg/ml) was used to permeabilize tissue sections. Sections were then incubated with nucleotide mix and rTdT enzyme at 37°C for 60 minutes. As a negative control sections without the rTdT enzyme were used. The sections were mounted in VECTASHIELD® + DAPI (Vector Lab Cat. H-1200) to stain nuclei and immediately analyzed under a fluorescence microscope Nikon Ti-E Perfect Focus System using a standard fluorescein filter set to view the green fluorescence of fluorescein at 520 ± 20 nm and blue DAPI at 460 nm under a 10x objective. All the nuclei of osteocytes (both live DAPI at 460 nm and dead green fluorescein at 520 nm) were counted with ImageJ software using particle analysis in the Nucleus counter plugin. All the dead cells were quantified counting only green fluorescein nuclei with ImageJ software using particle analysis in the Nucleus counter plugin. From each site a representative area of 0.1 mm² (about 380x280 µm) was analysed from the surface of four different anatomical regions (condyle, condylar groove, sagittal ridge and fracture site).

Immunohistochemistry Frozen sections were labelled with Rb pAb Sclerostin (Ab63097, Abcam), Rb pAb HtrA1 (Ab38611, Abcam), Ms mAB Cathepsin K (Ab66267, Abcam) and Ms mAb MMP13 (Ab3208, Abcam) using

anti-Mouse IgG (071M6210, Sigma) and anti-Rabbit IgG (B8895, Sigma) secondary antibodies. A horse-radish peroxidase detection (HRP) method was used to detect staining and sections were then counter stained with Toludine Blue or Methyl Green to allow visual identification of the cells. Sections were examined using bright field optics on a Leica DMRXA2 with a QImaging Retiga EX fast 1394 camera system under a x60 and x100 objective. At each of the anatomical sites, the total number of osteocytes and the positively labelled osteocytes were quantified in an area of 1 mm^2 in the subchondral bone (immediately beneath the cartilage/bone interface, ('surface zone') and in an area of 1 mm^2 immediately below this ('deep zone') 5 to 10 mm below surface zone.

Statistics All samples were processed in order to collect four technical replicates for each experiment and the data are presented as the mean ± standard deviation (SD) with the significance level set at 0.05. The data were evaluated using Student's t test, ANOVA and non-parametric Mann-Whitney to determine statistically significant differences with GraphPad Prism 5 software.

Results

Microdamage quantification

In order to visualize the microdamage within the bones, the whole bone was stained prior to sectioning. This was done to ensure that damage produced during the processing would not be stained and would therefore be excluded from damage quantification (23, 25).

This study identified both microcracks and diffuse damage in the samples studied (Figure 3). There was significantly increased microcrack damage/area in the lateral condyle fracture site of Group F (7.04 +\- 2.91 cracks/mm^2) compared to the contralateral limb (Group CL) (3.18 +\- 4.26 cracks/mm^2) and the control horses (Group C) (2.93 +\- 3.85 cracks/mm^2), p=0.002 and p=0.005, respectively. When the total microcrack damage was compared for the other 3 sites there was no significant difference between sites. There was no significant difference between experimental groups at any site in the amount of diffuse damage/area with Group F having 3.43 +\- 1.5 discrete areas of staining compared to 2.92 +\- 1.45 in Group CL and 2.55 +\- 1.67 in Group C.

Quantification of apoptosis

The DeadEnd fluorometric apoptosis analysis detected apoptotic cells in all samples studied (Figure 4). When data from all 4 sites was pooled, there were significantly fewer apoptotic osteocytes in Group F compared to Group CL (p=0.002) but no difference in the percentage apoptotic osteocytes recorded

when comparing with raced horses (Group F + CL) and Group C. The difference was greatest on the sagittal ridge where the rate of apoptotic cells was 22.2±11.0% in Group F compared to 47.0±19.6% in Group CL (p=0.007).

Enzyme Immunohistochemistry

MMP-13, HtrA1 and Cathepsin K immunoreactivity was detected in all samples studied. Positive staining was detected in the cytoplasm of the osteocytes in the bone. MMP-13, HtrA1 and Cathepsin K immunoreactivity was not different among groups or anatomical sites (Figure 5).

Sclerostin immunolocalisation

Sclerostin immunoreactivity was detected in all samples studied (Figure 6). Positive staining was detected in the cytoplasm of the osteocytes in the bone. No staining was detected in the cartilage or within the blood vessels. No differences between sites was detected except in the lateral condylar fracture site groove. At this site sclerostin immunohistochemistry showed that, in the subchondral bone under the articular surface ('surface zone') staining was in the range of 3.9+/- 2.9% of osteocytes staining positive for sclerostin in all samples studied. In the deep zone however, sclerostin immunohistochemistry showed that there was a significant increase in positive staining in Group F compared to Group CL, with a mean of 24.4 +/- 19.4% of osteocytes staining positive for sclerostin (p=0.03) (Figure 7).

Discussion

In this study we have shown that osteocyte apoptosis is not increased in regions of microdamage in the MCIII of TB racehorses in California that sustain fatal lateral condylar fractures. We have demonstrated increased levels of a wnt signalling inhibitor protein, sclerostin, associated with the fracture line in the fractured bones, but no evidence of osteocytic osteolysis in these samples. Our results suggest that wnt signalling pathways may be important in the aetiopathogenesis of microdamage induced stress fracture in the TB racehorse.

Microdamage has been documented in numerous TB racehorse fractures as evidence of pre-fracture pathology (26, 27). In this study we confirmed that our samples had microdamage similar to that reported in previous studies by pre-sectioning staining of the samples with acid Fuchsin, ensuring that the microdamage identified was not caused by sample preparation (24). We identified a mean of 7.04 +/- 2.91 microcracks/mm^2 joint surface in fractured bones, which is consistent with a previous report (22), and indicated that the samples included in the study were representative of stress induced microdamage as reported previously in the literature.

It has long been proposed that the development of linear fracture microcracks through repetitive experimental loading is associated with a loss of osteocyte

viability in the region of the microcrack and the areas that subsequently formed resorption spaces (28, 29). These, and other, observations led to the concept that the osteocyte has a role as a mechanoreceptor in bone, sensing load and regulating bone adaptation (16). A number of small animal *in* vivo studies have demonstrated that, in these acute models (7-10d experiments), osteocytes regulate bone formation through an apoptosis-mediated mechanism (30-32). This mechanism is currently considered to underlie the control targeted remodelling of microdamage. However, these acute small animal experiments, primarily conducted in the rat ulnar fatigue damage model, evaluate very different events compared to the chronic, high velocity overloading of the McIII experienced by the TB racehorse and may underlie why, in this study, the naturally occurring microdamage is not associated with osteocyte apoptosis. Our observations agree with previous studies in the equine distal MCIII. In other studies, no association between targeted remodelling and osteocytes apoptosis has been demonstrated (8, 33). Taken together these studies suggest that targeted remodelling in the racehorse is not dependent on osteocyte apoptosis, but that an alternative mechanism of regulation may be involved.

In the rat ulnar model of microdamage, it has been hypothesised that osteocyte apoptosis stimulates bone remodelling initially via osteoclastic resorption (34). However, osteocytes can regulate bone remodelling via other mechanisms, for example by osteocytic osteolysis and wnt-signalling

pathways (35). In osteocytic osteolysis osteocytes directly resorb their surrounding environment via a cathepsin K and/or MMP13 associated mechanism (36, 37). In this study we did not find an association between Cathepsin K, MMP13 or HtrA1 immunoreactivity and bone damage, suggesting that osteocytic osteolysis through Cathepsin K, MMP13 or HtrA1 pathways is not linked to microdamage in the racehorse.

In contrast, however, there was evidence for an association between the wnt signalling pathway and microdamage. Osteocytes regulate bone formation primarily via their production of the wnt signalling protein sclerostin, that inhibits bone formation (15) and responds to local load (16). In this study we identified sclerostin protein in osteocytes in all samples studied, however, we detected a marked and significant increase in sclerostin positive osteocytes along the fractured line. This finding of increased sclerostin in the region of the fracture was unexpected; in rat ulnar models of stress fracture sclerostin has been reported as reduced adjacent to the fracture line (38), albeit over the short time courses of the experiment. However, in association with the finding that osteocyte apoptosis is not associated with equine microdamage but is with rat ulnar microdamage, these results indicate that microdamage in the racehorse may have a fundamentally different pathological process to that modelled in small animals.

The presence of increased sclerostin associated with an overt fracture line in these cases of equine stress fracture is intriguing. One explanation is that the increase in sclerostin is a direct result of increased bone density at the site of the microdamage and that sclerostin – an inhibitor of bone formation - is being produced locally to prevent further, supra-physiological bone mass increases which causes increased stiffness and likelihood of fracture. Racehorse training does cause increased bone density in the distal Mc-III (39, 40) and this bone density has been shown to be heterogenous across the distal Mc-III (40-42). It has been suggested that these bone density gradients within the bone further drive the formation of microdamage. The observation that sclerostin is increased at the site of fracture might suggest that sclerostin is being upregulated here to inhibit 'excessive' bone formation prevent worsening bone density gradients that may ultimately lead to overt fracture. However, the fact that the increased sclerostin was only seen in the overtly fractured bones, rather than in the contralateral limb which has experienced similar racing and training, indicates that the increased sclerostin could be an end stage event associated with high probability of fracture. Sclerostin is upregulated by unloading of bone ('stress shielding') (43, 44), it may be that local unloading caused by heterogenous bone density changes is acting as the mechanism to drive this increased sclerostin expression. The possibility that sclerostin might play a role in reducing the physiological consequences of 'excessive bone' mass has also been suggested by the finding that constitutive activation of osteocyte β-catenin in mice increased bone mass

(38), but led to significantly increased serum sclerostin levels, suggested by these authors to be a protective mechanism.

There are a number of limitations with this study. One limitation is that the samples studied do not allow an accurate determination of when the observed increase in sclerostin occurred relative to the fracture. The observed increase in sclerostin could have been produced prior to fracture, between fracture and death or, less likely, post mortem. The horses included in this study were euthanased within 10 minutes of fracture occurring, which compares favourably with the longer time between naturally occurring fracture and bone sample acquisition in similar studies in man (fractured neck of femur). However, it has been shown that sclerostin levels in fracture haematoma are significantly increased compared to serum levels, indicating that sclerostin is indeed induced by fracture (45) and future studies should ensure extremely rapid collection and fixation of samples prior to processing.

Another limitation of this study is that sclerostin was only investigated in the distal metacarpus. Further work is required to investigate fractures at other anatomical sites and also to investigate any relationship between the levels of training/racing undergone by the horse and sclerostin levels.

In conclusion, this study finds no evidence for a role of osteocyte apoptosis or osteocytic osteolysis in the stress fractures of Mc-III of the TB racehorse. However, a marked increase in the wnt signalling inhibitor sclerostin was

detected, suggesting that this protein may be produced to reduce further bone deposition as an end stage event in a bone that has remodelled too far to sustain its integrity.

References

1. Parkin TD, Clegg PD, French NP, Proudman CJ, Riggs CM, Singer ER, et al. Risk of fatal distal limb fractures among Thoroughbreds involved in the five types of racing in the United Kingdom. The Veterinary record. 2004;154(16):493-7.
2. Dyson PK, Jackson BF, Pfeiffer DU, Price JS. Days lost from training by two- and three-year-old Thoroughbred horses: a survey of seven UK training yards. Equine veterinary journal. 2008;40(7):650-7.
3. Owen KR, Dyson SJ, Parkin TD, Singer ER, Kristoffersen M, Mair TS. Retrospective study of palmar/plantar annular ligament injury in 71 horses: 2001-2006. Equine veterinary journal. 2008;40(3):237-44.
4. Radtke CL, Danova NA, Scollay MC, Santschi EM, Markel MD, Da Costa Gomez T, et al. Fatigue fracture of the condyles of the third metacarpal/third metatarsal bone in Thoroughbred racehorses. Am J Vet Res. 2003;64:1110-6.
5. Boyde A, Haroon Y, Jones SJ, Riggs CM. Three dimensional structure of the distal condyles of the third metacarpal bone of the horse. Equine veterinary journal. 1999;31(2):122-9.
6. Nunamaker DM, Butterweck DM, Provost MT. Fatigue fracrture in thoroughbred racehorses: relationships with age, peak bone strain and training. J Orthop Res. 1990;8:604-11.
7. Muir P, McCarthy J, Radtke CL, Markel MD, Santschi EM, Scollay MC, et al. Role of endochondral ossification of articular cartilage and functional adaptation of the subchondral plate in the development of fatigue microcracking of joints. Bone. 2006;38:342-9.
8. Muir P, Peterson AL, Sample SJ, Scollay MC, Markel MD, Kalscheur VL. Exercise-induced metacarpophalangeal joint adaptation in the Thoroughbred racehorse. J Anat. 2008;213:706-17.
9. Vakil JJ, O'Reilly MP, Sutter EG, Mears SC, Belkoff SM, Khanuja HS. Knee arthrotomy repair with a continuous barbed suture: a biomechanical study. The Journal of arthroplasty. 2011;26(5):710-3.
10. Kawcak CE NR, McIlwraith CW, Trotter GW. Sucbchondral bone reaction to exercise. AAEP Proceedings 1999(45):2.
11. Bentley VA, Sample SJ, Livesey MA, Scollay MC, Radtke CL, Frank JD, et al. Morphologic changes associated with functional adaptation of the navicular bone of horses. Journal of anatomy. 2007;211(5):662-72.

12. Burr DB. Targeted and nontargeted remodeling. Bone. 2002;30:2-4.
13. Bonewald LF. The amazing osteocyte. J Bone Min Res. 2011;26:229-38.
14. Schaffler MB, Kennedy OD. Osteocyte signalling in bone. Curr Osteoporos Res. 2012;10:116-25.
15. Larsson S. Anti-sclerostin - is there an indication? Injury. 2016;47 Suppl 1:S31-5.
16. Nguyen J, Tang SY, Nguyen D, Alliston T. Load regulates bone formation and Sclerostin expression through a TGFβ-dependent me. PLoS One. 2013;8:e53813.
17. Ominsky MS, Li C, Li X, Tan HL, Lee E, Barrero M, et al. Inhibition of sclerostin by monoclonal antibody enhances bone healing and improves bone density and strength of nonfractured bones. Journal of bone and mineral research : the official journal of the American Society for Bone and Mineral Research. 2011;26(5):1012-21.
18. Li C, Ominsky MS, Tan HL, Barrero M, Niu QT, Asuncion FJ, et al. Increased callus mass and enhanced strength during fracture healing in mice lacking the sclerostin gene. Bone. 2011;49(6):1178-85.
19. Wysolmerski JJ. Osteocytes remove and replace perilacunar mineral during reproductive cycles. Bone. 2013;54:230-6.
20. Tang SY, Herber RP, Ho SP, Alliston T. Matrix metalloproteinase-13 is required for osteocytic perilacunar remodelling and maintains bone fracture resistance. J Bone Min Res. 2012;27:1936-50.
21. Tsuchiya A, Yano M, Tocharus J, Kojima H, Fukomoto M, Kawaichi M, et al. Expression of mouse HtrA1 serine protease in normal bone and cartilage and its upregulation in joint cartilage damaged by experimental arthritis. Bone. 2005;37:323-36.
22. Riggs CM, Whitehouse GH, Boyde A. Structural variation of the distal condyles of the third metacarpal and third metatarsal bones in the horse. Equine veterinary journal. 1999;31(2):130-9.
23. Muir P, Peterson AL, Sample SJ, Scollay MC, Markel MD, Kalscheur VL. Exercise-induced metacarpophalangeal joint adaptation in the Thoroughbred racehorse. Journal of anatomy. 2008;213(6):706-17.
24. Bentolila V, Boyce TM, Fyhrie DP, Drumb R, Skerry TM, Schaffler MB. Intracortical remodeling in adult rat long bones after fatigue loading. Bone. 1998;23(3):275-81.
25. Burr DB, Hooser M. Alterations to the en bloc basic fuchsin staining protocol for the demonstration of microdamage produced in vivo. Bone. 1995;17(4):431-3.
26. van Oers RF, van Rietbergen B, Ito K, Huiskes R, Hilbers PA. Simulations of trabecular remodeling and fatigue: is remodeling helpful or harmful? Bone. 2011;48(5):1210-5.
27. Vallance SA, Spriet M, Stover SM. Catastrophic scapular fractures in Californian racehorses: pathology, morphometry and bone density. Equine veterinary journal. 2011;43(6):676-85.

28. Bentolila V, Boyce TM, Fyhrie DP, Drumb R, Skerry TM, Schaffler MB. Intracortical remodeling in adult rat long bones after fatigue loading. Bone. 1998;23:275-9.
29. Verborgt O, Gibson GJ, Schaffler MB. Loss of osteocyte integrity in association with microdamage and bone remodelling after fatigue in vivo. J Bone Min Res. 2000;15:60-70.
30. Cardoso L, Herman BC, Verborgt O, Laudier DM, Majeska RJ, Schaffler MB. Osteocyte apoptosis controls activation of intracortical resorption in response to bone fatigue. J Bone Miner Res. 2009;24:597-605.
31. Noble BS, Peet N, Stevens HY, Brabbs A, Mosley JR, Reilly GC, et al. Mechanical loading:biphasic osteocyte survival and targetting of osteoclasts for bone destruction in rat cortical bone. Am J Physiol Cell Physiol. 2003;284:C934-43.
32. Vashishth D, Verborgt D, Divine G, Schaffler MB, Fyhrie DP. Decline in osteocyte lacunar density in human cortical bone is associated with accumulation of microcracks with age. Bone. 2000;26:375-80.
33. Da Costa Gómez TM, Barrett JG, Sample SJ, Radtke CL, Kalscheur VL, Lu Y, et al. Up-regulation of site-specific remodeling without accumulation of microcracking and loss of osteocytes. Bone. 2005;37:16-24.
34. Kennedy OD, Herman BC, Laudier DM, Majeska RJ, Sun HB, Schaffler MB. Activation of resorption in fatigue-loaded bone involves both apoptosis and active pro-osteoclastogenic signaling by distinct osteocyte populations. Bone. 2012;50(5):1115-22.
35. Prideaux M, Findlay DM, Atkins GJ. Osteocytes: The master cells in bone remodelling. Current opinion in pharmacology. 2016;28:24-30.
36. Tang SY, Herber RP, Ho SP, Alliston T. Matrix metalloproteinase-13 is required for osteocytic perilacunar remodeling and maintains bone fracture resistance. Journal of bone and mineral research : the official journal of the American Society for Bone and Mineral Research. 2012;27(9):1936-50.
37. Qing H, Ardeshirpour L, Pajevic PD, Dusevich V, Jahn K, Kato S, et al. Demonstration of osteocytic perilacunar/canalicular remodeling in mice during lactation. Journal of bone and mineral research : the official journal of the American Society for Bone and Mineral Research. 2012;27(5):1018-29.
38. Tu X, Delgado-Calle J, Condon KW, Maycas M, Zhang H, Carlesso N, et al. Osteocytes mediate the anabolic actions of canonical Wnt/beta-catenin signaling in bone. Proceedings of the National Academy of Sciences of the United States of America. 2015;112(5):E478-86.
39. Riggs CM, Boyde A. Effect of exercise on bone density in distal regions of the equine third metacarpal bone in 2-year-old thoroughbreds. Equine veterinary journal Supplement. 1999(30):555-60.
40. Loughridge AB, Hess AM, Parkin TD, Kawcak CE. Qualitative assessment of bone density at the distal articulating surface of the third metacarpal in Thoroughbred racehorses with and without condylar fracture. Equine veterinary journal. 2015.
41. Stover SM, Murray A. The California Postmortem Program: leading the way. Vet Clin North Am Equine Pract. 2008;24(1):21-36.

42. Ramzan PH, Powell SE. Clinical and imaging features of suspected prodromal fracture of the proximal phalanx in three Thoroughbred racehorses. Equine veterinary journal. 2010;42(2):164-9.
43. Lin C, Jiang X, Dai Z, Guo X, Weng T, Wang J, et al. Sclerostin mediates bone response to mechanical unloading through antagonizing Wnt/beta-catenin signaling. Journal of bone and mineral research : the official journal of the American Society for Bone and Mineral Research. 2009;24(10):1651-61.
44. Spatz JM, Wein MN, Gooi JH, Qu Y, Garr JL, Liu S, et al. The Wnt Inhibitor Sclerostin Is Up-regulated by Mechanical Unloading in Osteocytes in Vitro. The Journal of biological chemistry. 2015;290(27):16744-58.
45. Sarahrudi K, Thomas A, Albrecht C, Aharinejad S. Strongly enhanced levels of sclerostin during human fracture healing. Journal of orthopaedic research : official publication of the Orthopaedic Research Society. 2012;30(10):1549-55.

Figure legends

Figure 1. Dorso-palmar radiographs of intact third metacarpal bone (A) and contralateral, fractured bone of same horse (B). Photograph of articular surfaces of intact bone (C) and contralateral fractured third metacarpal bone (D).

Figure 2. Dorso-palmar radiographs of fractured third metacarpal bone (A) and contralateral bone (B). The different regions used in the analysis of staining are shown. A = medial condyle, B = medial condylar groove, C = sagittal ridge and D = lateral condylar fracture site. In C the sampling site regions are shown, corresponding to A-D in B.

Figure 3. A to C representative micrographs of acid Fuchsin labelled structures in metacarpal bones. A) Linear microcrack extending from articular surface, B) staining around blood vessels, C) diffuse microdamage extending from articular surface. D) Amount of damage per surface area of section shown for microcracks and diffuse damage. There is no difference in the amount of diffuse damage quantified in the three groups, however there is a statistically significant difference between the amount of microcrack damage/surface area in the lateral condyle (site D) compared to both contralateral and control bones. Scale bar 100 μm. F = fractured bones, Cl = contralateral bones and C = control bones. $P<0.05$ and indicated by ***.

Figure 4. A) Quantification of apoptosis within osteocytes in non-fractured and fractured samples, B) Raced and non-raced samples and C) samples from the sagittal ridge. There is a statistically significant difference in the numbers of apoptotic cells ($p<0.05$) between non-fractured and fractured samples (A) and in the numbers of apoptotic cells on the sagittal ridge, with a significant increase in apoptotic cells in

the contralateral limb samples (C). No difference was recorded in the numbers of osteocytes in the samples (D and E). F) Representative microscope image of a fluorometric TUNEL apoptosis analysis. Blue stain shows live cell nuclei, green stain shows apoptotic cells. Scale bar 100 μm. F = fractured bones, CL = contralateral bones and C = control bones.

Figure 5. Representative photomicrographs of immunohistochemistry in osteocytes in the subchondral bone. A) MMP-13, B) Cathepsin K, C) HTrA1. Osteocytes stained positively are seen as black cells in the fractured samples. In A) the cartilage is stained with Toluidine Blue, in B) the cartilage is stained with methyl green. Scale bar 100 μm.

Figure 6. Representative photomicrographs of sclerostin immunohistochemistry. A) Subchondral bone area control sample, B) subchondral area fracture sample, C) deep zone control sample, D) deep zone fracture sample. Osteocytes (Arrowheads in A and C) stained positively for sclerostin are seen as black cells in B and D (Group F) and shown by black arrows. In A the cartilage is stained with Toluidine Blue. Scale bar 100 μm. c= cartilage, scb = subchondral bone. The cartilage is stained with Toluidine Blue and is visible in A and B. The fracture site is to the bottom of the figures in C and D (black arrowhead).

Figure 7. Quantification of sclerostin immunohistochemistry within osteocytes in fractured (F) and contralateral (CL) limbs. There is a significant increase (* $p<0.05$) in sclerostin immunoreactivity in the deep zone of the fractured bone. In the photograph the approximate site of the cartilage/bone interface region (white arrow) and the deeper region is indicated (black arrow).

584
585 Figure 1.
586

Figure 2.

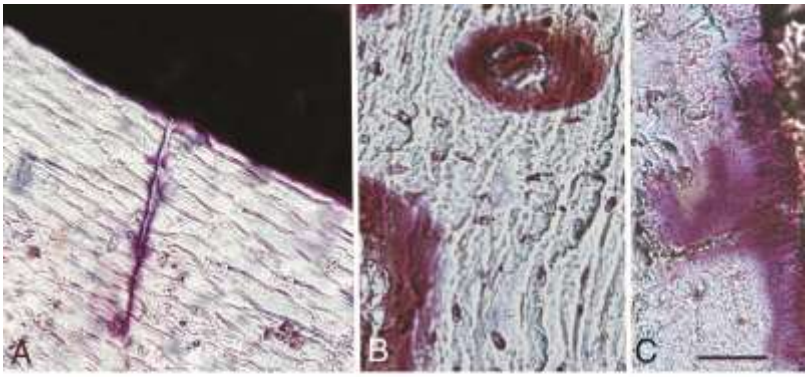

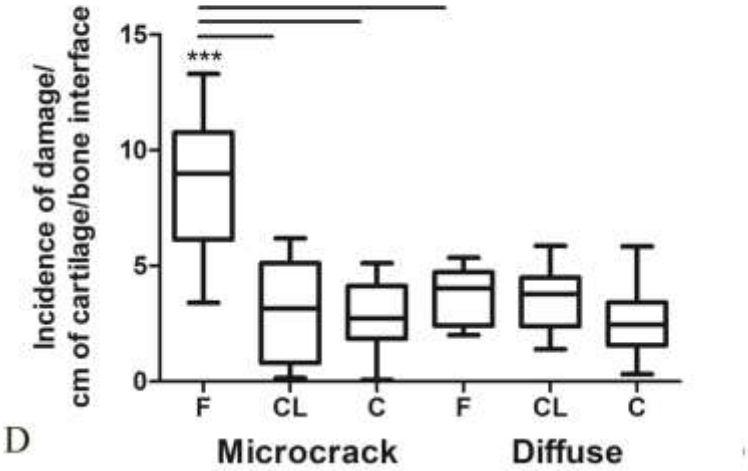

Figure 3.

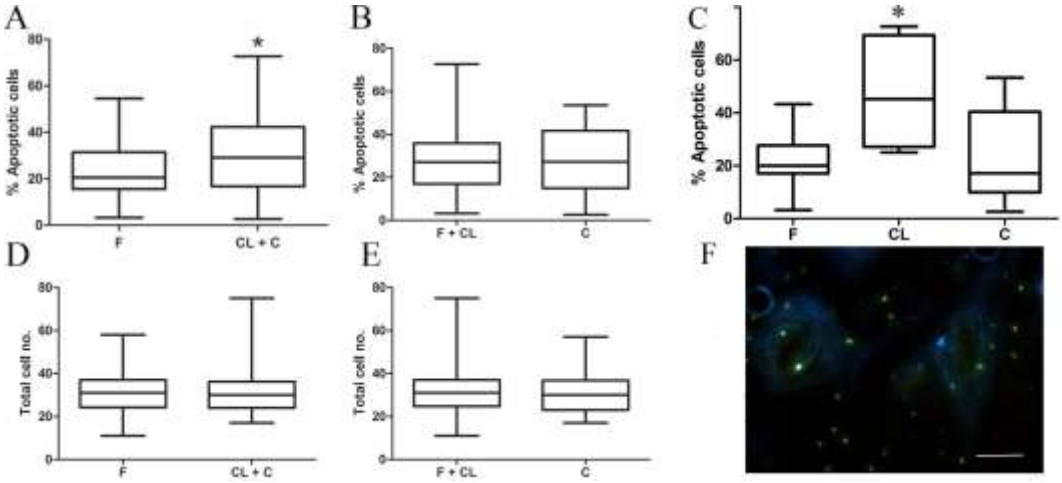

Figure 4.

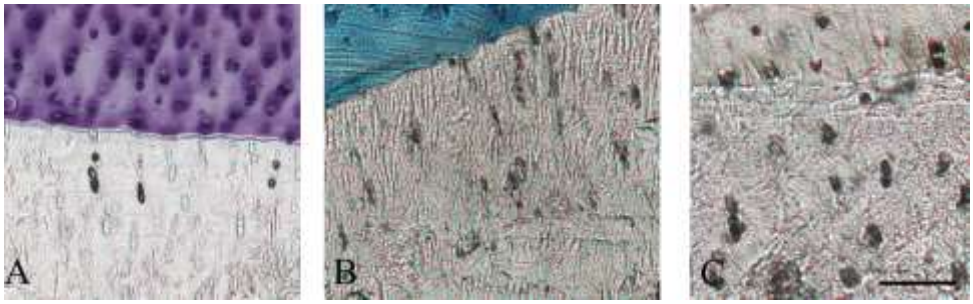

Figure 5.

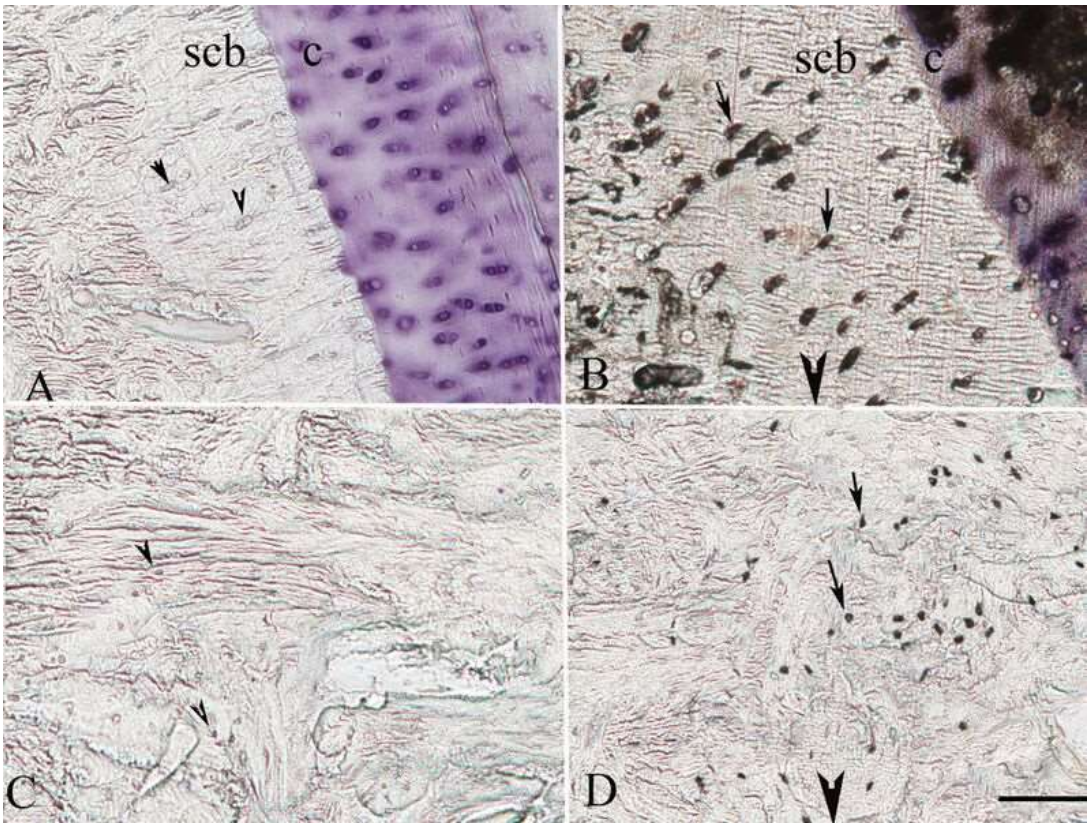

Figure 6.

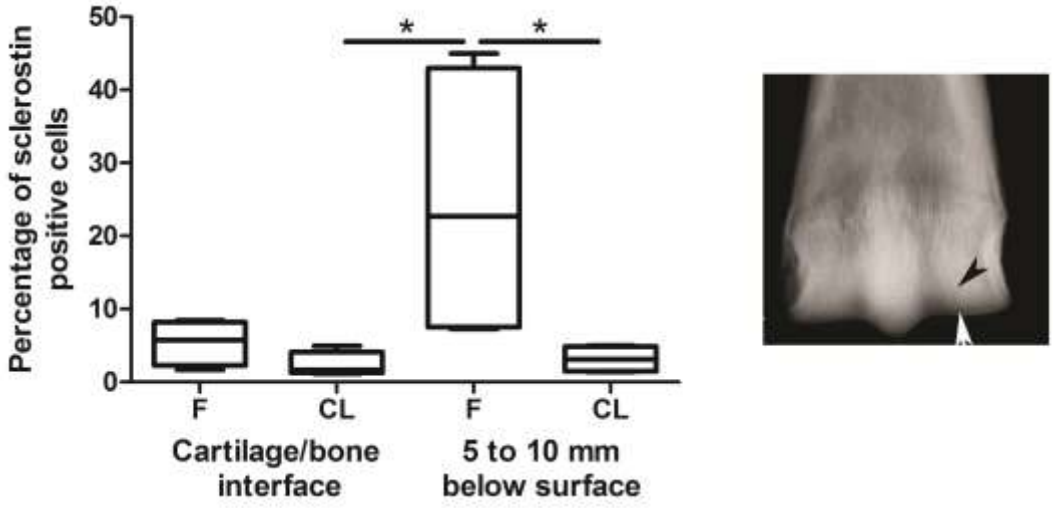

Figure 7.